Paper No.
11260

NACE INTERNATIONAL CORROSION 2011 CONFERENCE & EXPO

Prediction of Uniform CO_2 Corrosion of Mild Steel under Inert Solid Deposits

Jin Huang, Bruce Brown, Yoon-Seok Choi and Srdjan Nešić

Institute for Corrosion and Multiphase Technology
Department Of Chemical & Biomolecular Engineering
Ohio University
342 West State Street
Athens, OH 45701
USA

ABSTRACT

The effect of an inert solid deposit on uniform CO_2 corrosion of mild steel is modeled based on a mechanistic electrochemical CO_2 corrosion model. Laboratory testing has shown that the dominant factors introduced by the inert solids deposit are related to surface coverage, where both anodic and cathodic reaction rates are decreased because of less active surface area being exposed. The inert solid deposits also create a mass transfer barrier for corrosive species which limits the rate of the cathodic reactions. An existing mechanistic electrochemical model was modified to account for these effects and was capable of capturing the main features of uniform CO_2 corrosion of mild steel under inert solid deposits.

Key words: underdeposit, CO_2 corrosion, mild steel, model, mass transfer

INTRODUCTION

Severe crevice and pitting corrosion problems can be found under solid deposits in oil and gas pipelines[1]. Localized corrosion can occur under these deposits as they can provide an environment which is chemically and physically different than the areas which are uncovered. Such heterogeneities may lead to formation of galvanic corrosion cells, affect inhibitor performance or harbor bacterial growth leading to MIC[,[2],[3]]. Underdeposit corrosion is more prevalent at the bottom of horizontal lines and where flow rates are lowest. However, there are very few studies to be found in the open literature related to the mechanisms of underdeposit CO_2 corrosion[4]. Most of the available literature refers to the effect of deposits on corrosion inhibitor performance.[5] [-[8]] Since deposits have been reported as an important factor which may lead to severe CO_2 corrosion, it's very important to understand first the mechanisms of uniform corrosion under solid deposits, before focusing on the effect they have on corrosion inhibitor performance.

Real-life scenarios for under deposit CO_2 corrosion found in oil/gas pipelines are very complex. An *in situ* deposit is likely to be neither pure nor inert. Rather it has complex composition and even some reactivity. Typical deposits consist of combinations of inorganic solids such as sand, scale and corrosion products, and organic matter such as wax and inhibitor residues. In addition, oxygen (O_2), acetic acid (CH_3CO_2H), hydrogen sulfide (H_2S) and bacteria were found in some deposits.

In the present phase of the project on underdeposit corrosion, the initial step was made to measure and define the effect of pure and inert deposits on uniform CO_2 corrosion of mild steel. Then an effort to model the observed behavior was made using a simple mechanistic CO_2 corrosion model such as the one proposed by Nešić, *et al.* [4]

EXPERIMENTAL PROCEDURE

Experiment set up

Experiments were conducted at atmospheric pressure in a three-electrode glass cell, Figure 1. The cell was filled with 2 liters of 1 wt% NaCl solution. CO_2 was continuously bubbled through the cell. API# 5L-X65 mild steel was used as the working electrode (WE) for electrochemical measurements. Platinum wire was used as a counter electrode (CE) and a KCl saturated silver-silver chloride (Ag/AgCl) reference electrode (RE) was connected to the cell externally *via* a Luggin capillary. A glass pH electrode was immersed in the electrolyte to monitor the pH during the experiment. Hydrochloric acid (HCl) or sodium bicarbonate ($NaHCO_3$) was added to adjust the pH at the beginning of the test to desired value, which didn't change much throughout the duration of the test. The temperature was maintained within ± 1°C using a hot plate and a thermocouple with feedback control.

The corrosion process was studied using electrochemical techniques including linear polarization resistance (LPR), potentiodynamic sweeps (PDS) and electrochemical impedance spectroscopy (EIS). Electrochemical measurements were made using a Gamry† potentiostat under computer control.

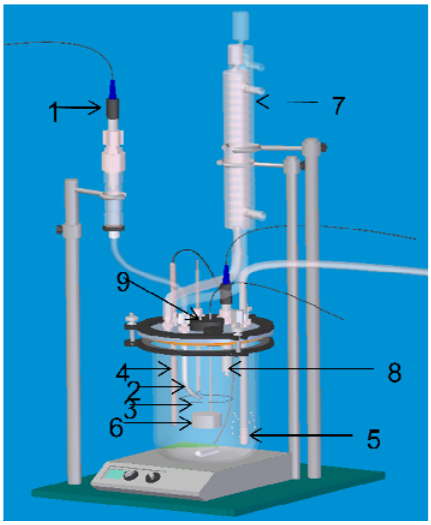

1. Reference Electrode
2. Luggin capillary
3. Platinum Counter Electrode
4. Temperature Probe
5. Sparger tube
6. Working Electrode (X65 carbon steel)
7. Condenser
8. pH meter
9. Deposit Inlet

Figure 1: Three-electrode glass cell apparatus.

† Trade Name
# American Petroleum Institute (API), 1220 L St. NW, Washington, DC 20005.

Material

Working electrode

X-65 mild steel, a typical pipeline material was used for all corrosion tests. The chemical composition of the steel is given in Table 1. The exposed area of the WE was 8.00 cm^2.

Table 1
Chemical composition of X65 mild steel (mass % balance is Fe) [9]

	C	Mn	Si	P	S	Cr	Cu	Ni	Mo	Al
X65	0.065	1.54	0.25	0.013	0.001	0.05	0.04	0.04	0.007	0.041

Solid deposit

Sand and SiO_2 powder were used as solid deposits in this work. Both of the deposits are the same base inorganic material, i.e. silica (SiO_2) sand. The main difference between them is their grain size and shape as can be seen in the SEM images shown in Figure 2. The properties of these deposits are listed in Table 2. The density and porosity of each type of deposit material was experimentally determined as previously reported.[10]

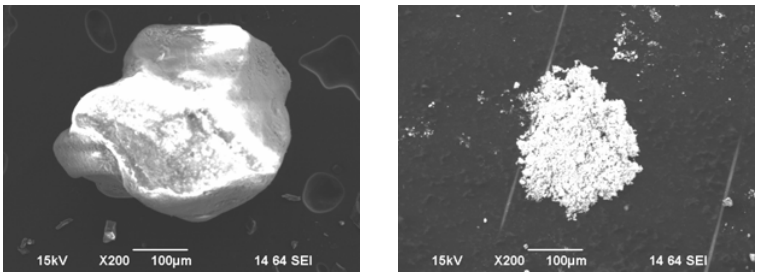

Sand SiO_2 powder

Figure 2: SEM images of deposit materials.

Table 2
Deposit properties

	Grain size	Bulk density*	Porosity#
SiO_2 powder	44 µm	0.75 g/cm^3	75%
sand	240 µm	2.5 g/cm^3	39%

* The mass of many particles of the material divided by the total volume they occupy.
\# The percentage of the volume of voids in a material composed of particles to the total volume the particles occupy.

Each deposit material was rinsed with DI water stored in a CO_2 purged solution similar to the test solution and transferred by pipette onto the tested sample shown in Figure 3.

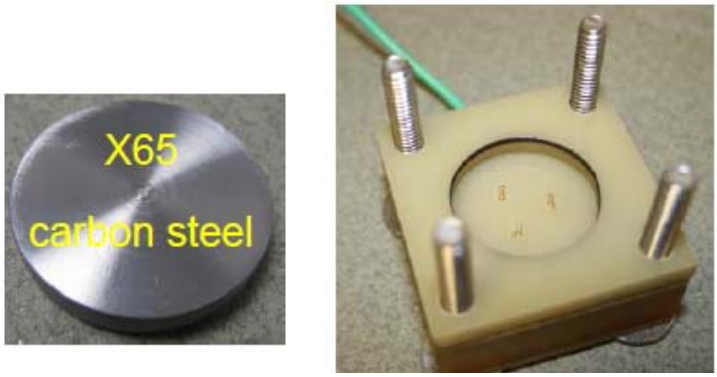

Figure 3: Corrosion sample and sample holder.

Procedure

In each experiment, CO_2 was bubbled through the electrolyte for a minimum of 60 minutes to saturate and deaerate the test solution.

The surface of the WE was sequentially polished using 200-, 400- and 600-grit silicon carbide paper, washed and rinsed with isopropyl alcohol before each experiment, mounted in the specimen holder and immersed into the electrolyte. The free corrosion potential measurement began immediately after the immersion and normally stabilized within ± 1 mV after 5 - 10 minutes.

Baseline "bare" steel corrosion tests were conducted at the same conditions as the under deposit corrosion tests. For each under deposit corrosion test, the test sample was immersed in the electrolyte for one hour without a deposit, where the free corrosion rate and solution resistance were measured by LPR and EIS respectively. The deposit was then introduced onto the WE steel surface and the test was further carried out for 24 hours.

The WE was polarized ±5 mV from open circuit potential (E_{oc}) during the LPR measurements at a scan rate of 0.125 mV/s to obtain the polarization resistance (R_p) which was then used to calculate the general corrosion rate of mild steel. For the EIS measurement, a sinusoidal potential signal ±5 mV peak-to-peak around E_{oc} was applied to the WE with scanning frequencies from 5 kHz to 1 mHz. This scan enables the identification of both the solution resistance (R_S) at the highest frequency range and a "fingerprint" of the various reactions involved in the corrosion process at the lower frequency ranges. The potentiodynamic sweeps were conducted at the end of each experiment by sweeping the potential at a scan rate of 0.125 mV/s in the cathodic (more negative) direction from E_{oc} to E_{oc}-0.4 V, and then disconnecting and pausing until a stable E_{oc} was attained, then the potential of the WE was swept in the anodic (more positive) direction from E_{oc} to E_{oc}+0.2 V using the same scan rate. Experimental conditions are summarized in Table 3. After each test, the WE surface morphology and composition were analyzed by SEM and EDX.

Table 3
Experimental conditions

Parameter	Conditions
Test material	X65 mild steel
Test solution	DI water + 1wt% NaCl
Temperature	25°C - 80°C
CO_2 partial pressure	0.54 bar - 0.96 bar
Solution pH	4 ~ 6
Deposit	Silica sand, SiO_2 powder
Deposit thickness	2 ~ 10 mm
Test duration	24 hour
Sweep rate	0.125 mV/s
Polarization resistance	From -5 mV to 5 mV vs. E_{oc}
EIS	±5 mV vs. E_{oc} from 5 kHz to 1 mHz
Potentiodynamic sweep	From -400 mV to +200 mV vs. E_{oc}

ELECTROCHEMICAL MODEL

The experimental observations led to the development of a mechanistic model for uniform CO_2 corrosion under inert solid deposits, first requiring consideration of the cathodic and anodic reactions involved.

Cathodic reactions

Initially CO_2 is hydrated to form carbonic acid in water:

$$CO_2 + H_2O \Leftrightarrow H_2CO_3$$

These species can then undergo partial dissociation:

$$H_2CO_3 \Leftrightarrow H^+ + HCO_3^-$$

$$HCO_3^- \Leftrightarrow H^+ + CO_3^{2-}$$

In CO_2 corrosion at a pH range of 4 to 6, the presence of CO_2 leads to a much higher corrosion rate than would be found in a solution of a strong acid at the same pH.[9] This is because the presence of dissolved CO_2 acts as a “reservoir” of carbonic acid and can help with replacement of consumed

hydrogen ions. Water reduction is also considered as one of the potential cathodic reactions in the present model. The three cathodic reactions considered in the model are:

$$H^+ + e^- \rightarrow H$$

$$H_2CO_3 + e^- \rightarrow H + HCO_3^-$$

$$H_2O + e^- \rightarrow H + OH^-$$

H^+ reduction

Generated current from hydrogen reduction ($H^+ + e^- \rightarrow H$) is calculated by the following equation[9]:

$$\frac{1}{i_{(H^+)}} = \frac{1}{i_{\alpha(H^+)}} + \frac{1}{i^d_{\lim(H^+)}} \quad \textbf{(1)}$$

where charge transfer current density ($i_{\alpha(H^+)}$) is:

$$i_{\alpha(H^+)} = \varepsilon \cdot i_{0(H^+)} \times 10^{-\frac{\eta}{b_c}} \quad \textbf{(2)}$$

$$\frac{i_{0(H^+)}}{i^{ref}_{0(H^+)}} = \exp\left(-\frac{\Delta H_{(H^+)}}{R}\left(\frac{1}{T} - \frac{1}{T_{ref}}\right)\right) \quad \textbf{(3)}$$

$$b_c = 2.303\frac{RT}{0.5F} \quad \textbf{(4)}$$

$$\eta = E - E_{rev} \quad \textbf{(5)}$$

T_{ref} = 25°C. R is gas constant R = 8.315 J/mol/K. F is Faraday constant, F = 96485 C/equiv.

Diffusion limiting current density is usually defined as:

$$i^d_{\lim(H^+)} = k_{m,eff} F[H^+]_b \quad \textbf{(6)}$$

where $k_{m,eff}$ is the mass-transfer coefficient and is calculated to take into account the flow effect on diffusion of species through the hydrodynamic boundary layer[9]. However, in this work, all tests were conducted in stagnant condition with the diffusion of species impeded primarily by the presence of inert solid deposit [10]. In the first approximation, the permeability (κ) of the surface deposit layer for transport of species depends on the superficial porosity ε and the shape and connectivity between the pores, expressed via the tortuosity ψ :

$$\kappa = \psi\varepsilon \quad \textbf{(7)}$$

It was found that the superficial porosity can be approximated with volumetric porosity [9] and the tortuosity can be related to porosity, so in the in the present work we can replace the mass transfer coefficient with:

$$k_{m,eff} = \frac{D_{H^+} \cdot \varepsilon^{1.3}}{L} \tag{8}$$

where L is deposit thickness.

Other parameters in the above equations are: [12]

Symmetry factor (at 25°C):

$$\alpha_c = 0.5$$

Exchange current density:

$$\frac{\partial \log i_{0(H^+)}}{\partial pH} = -0.5 \tag{9}$$

Reversible potential:

$$E_{rev(H^+)} = -\frac{2.303RT}{F} pH - \frac{2.303RT}{2F} \log p_{H_2} \tag{10}$$

H_2CO_3 reduction

The current density contributed by H_2CO_3 reduction is derived in a similar way as for H^+ reduction:

$$\frac{1}{i_{(H_2CO_3)}} = \frac{1}{i_{\alpha(H_2CO_3)}} + \frac{1}{i^r_{\lim(H_2CO_3)}} \tag{11}$$

$$i_{\alpha(H_2CO_3)} = \varepsilon \cdot i_{0(H_2CO_3)} \times 10^{-\frac{\eta}{b_c}} \tag{12}$$

At stagnant conditions, the chemical reaction limiting current density $i^r_{\lim(H_2CO_3)}$ is related to diffusion coefficient[9] and is found to be related to deposit thickness and effective diffusion coefficient as:

$$i^r_{\lim(H_2CO_3)} = F \cdot C_{CO_2} \cdot (K_{hyd} k^f_{hyd} D_{eff} L^{-1})^{0.5} \tag{13}$$

where the equilibrium constant for the CO_2 hydration reaction is $K_{hyd} = 2.58 \times 10^{-3}$ [9]. k^f_{hyd} is the forward reaction rate for the CO_2 hydration reaction. It is a function of temperature, and is calculated by using the following equation[11]:

$$k^f_{hyd} = 10^{169.2 - 53.0 \log T - \frac{11.715}{T}} \tag{14}$$

The effect of the deposit is expressed in the effective diffusion coefficient as:

$$D_{eff} = D \cdot \varepsilon^{1.3} \tag{15}$$

and

$$C_{CO_2,b} = k^d_{CO_2} \times p_{CO_2} \tag{16}$$

Where $k^d_{CO_2}$ is Henry's constant and is a function of temperature:[12]

$$k^d_{CO_2} = 0.0454(1.6616 - 5.736\times10^{-2}t + 1.031\times10^{-3}t^2 \\ -9.68\times10^{-6}t^3 + 4.471\times10^{-8}t^4 - 7.912\times10^{-11}t^5) \tag{17}$$

H_2O reduction

Since water is considered to be present in "unlimited" quantities at the metal surface, it is then assumed that water reduction is limited by a charge-transfer process and the Tafel equation applies:

$$i_{H_2O} = \varepsilon \cdot i_{0,H_2O} \times 10^{-\frac{\eta}{b_c}} \tag{18}$$

It was determined experimentally[10] that the exchange current density for water reduction is $i_{0,H_2O} \approx 3\times10^{-5}\,\mathrm{A/m^2}$.

Anodic reaction

Iron dissolution in water is the only reaction considered for the anodic contribution:

$$Fe \rightarrow Fe^{2+} + 2e^-$$

From experimental observation[12] iron dissolution is under charge transfer control:

$$i_{Fe} = \varepsilon \cdot i_{0,Fe} \times 10^{\frac{\eta}{b_a}} \tag{19}$$

where,

$$\frac{i_{0,Fe}}{i_{0,Fe}{}^{ref}} = \exp\left(-\frac{\Delta H_{(Fe)}}{R}\left(\frac{1}{T} - \frac{1}{T_{ref}}\right)\right) \tag{20}$$

$T_{ref} = 20^{\circ}C$, $\Delta H_{(Fe)} = 40\mathrm{KJ/mol}$ $i_{0,Fe}{}^{ref} = 1\ \mathrm{A/m^2}$ and b_a = 40 mV[12].

RESULTS

Detailed experimental results have been presented and discussed in a previous publication[10]. It was concluded there that the effect of inert solid deposit on CO_2 corrosion of mild steel was a combination of a surface coverage effect and a mass transfer effect. The surface coverage effect is due to the direct contact of sand with the metal surface reducing the amount of metal surface area available for corrosion, thus reducing the magnitude of both anodic and cathodic reactions. Available metal surface area was directly proportional to deposit porosity. The mass transfer effect was related to the depth of the deposit and the porosity and tortuosity of the path for diffusion of species to the steel surface. These results will be compared below with the predictions made by the model described above.

MODEL VERSUS EXPERIMENTS

The underdeposit CO_2 corrosion was first tested for a bare steel corrosion condition. Figure 4 is the comparison of a potentiodynamic sweep predicted from the present model with experimental data. It can be seen that the anodic and cathodic portions of the potentiodynamic sweep capture the corrosion processes very well and the prediction is in good agreement with the experiment.

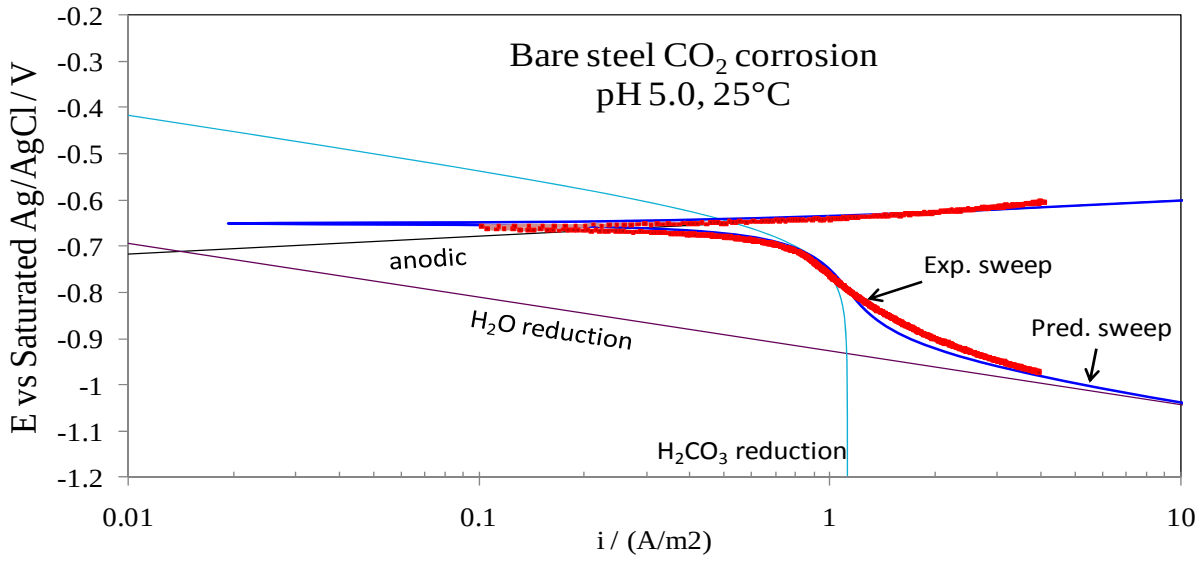

Figure 4: CO_2 corrosion of bare X65 steel at pH 5, 25°C, 1 wt% NaCl solution, $p_{CO_2} = 0.96$ bar.

The effect of deposit porosity

In Figure 5, anodic and cathodic potentiodynamic sweeps conducted on X65 mild steel covered by a 2 mm deposit of either SiO_2 powder or sand are contrasted with those conducted on bare steel at bulk solution pH 5 and 25°C. Experimental results are in good agreement with the predictions of individual reactions generated with the present model. Both anodic and cathodic reactions are diminished with the decrease in deposit porosity. The relatively small decrease in the anodic current stems from the decrease in the available metal surface (by coverage). The decrease in the cathodic current is predominantly because of the increased difficulty in the diffusion of corrosive species involved in the cathodic reactions.

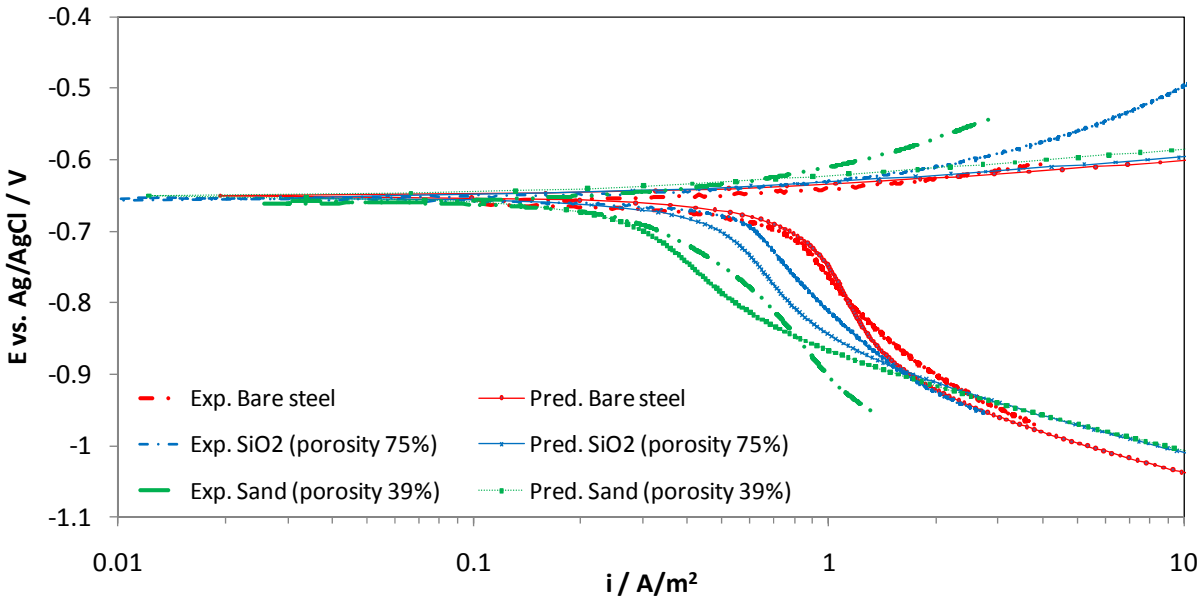

Figure 5: Effect of deposit porosity on CO_2 corrosion of X65 steel at pH 5, 25 °C, 1 wt% NaCl solution, $p_{CO_2} = 0.96$ bar, 2 mm deposit.

The effect of deposit thickness

Anodic and cathodic potentiodynamic sweeps conducted for an X65 mild steel surface covered with different sand depths are compared with those conducted on bare steel at bulk solution pH 5 and 25°C. With the change in the deposit thickness, the anodic current did not change substantially as can be seen in Figure 6. This is because increasing the deposit thickness only increases the mass transfer resistance of corrosive species for cathodic reactions. The measured potentiodynamic sweeps are in good agreements with the prediction. The thicker the deposit is the more tortuous the path of diffusion for species to go through, which results in a smaller cathodic current.

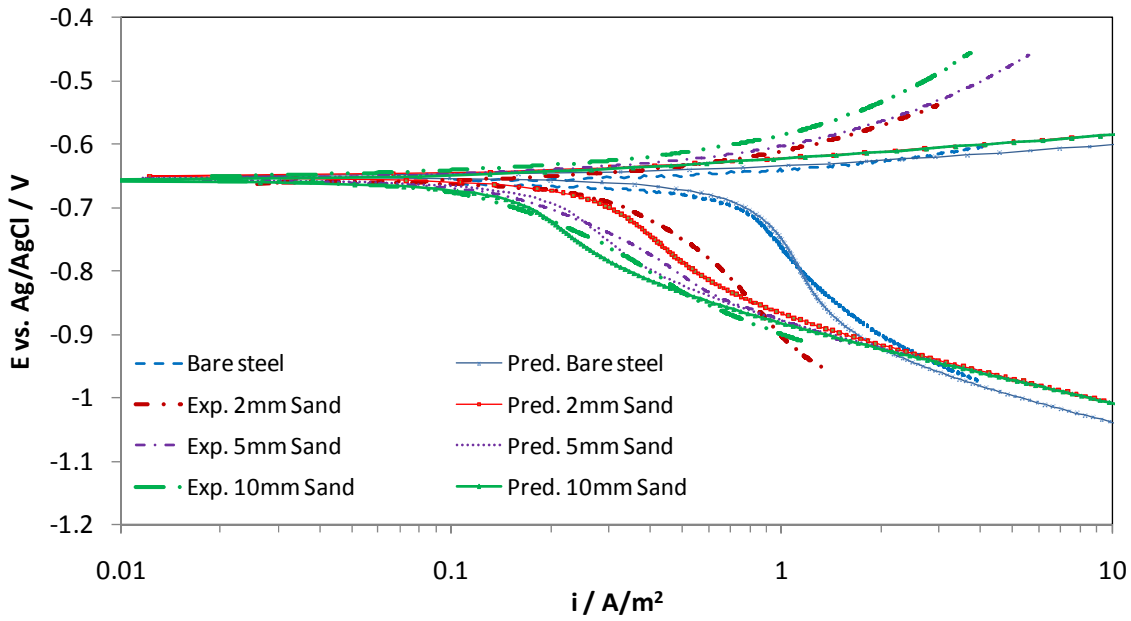

Figure 6: Deposit thickness effect at pH 5, 25 °C, 1 wt% NaCl solution, $p_{CO_2} = 0.96$ bar, sand porosity = 39%.

Temperature effect

Anodic and cathodic potentiodynamic sweeps on X65 mild steel covered with a 10 mm sand deposit were conducted at 25°C and 80°C (Figure 7). The corrosion rate of mild steel under this type of deposit did not increase with increasing temperature as would be observed in bare steel corrosion. However, some iron carbonate crystals were observed on the metal surface under the deposit which was not seen in bare steel corrosion.

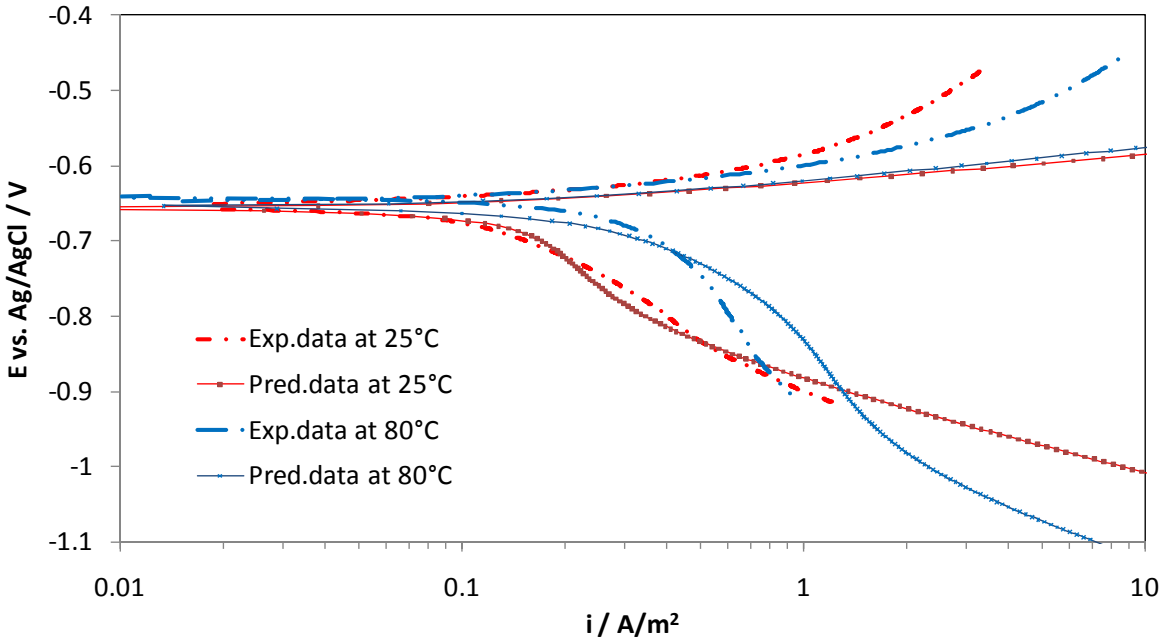

Figure 7: Temperature effect at pH 5, 1 wt% NaCl solution, 25 °C and 80 °C, 10 mm sand deposit (porosity = 39%).

Corrosion rate prediction

The general corrosion rates predicted by the present model were compared with experimental measurements using LPR. Figure 8 compares the corrosion rate for different porosities, and Figure 9 is for different deposit thickness. The B value used in calculating corrosion rate from LPR data was 13 mV. The prediction of corrosion rate at 25°C is in good agreement with the experimental results. However, the one at 80°C differs from the one measured from LPR, see Figure 10. The difference could be due to the use of an inappropriate B value in the LPR calculation at 80°C and due to formation of iron carbonate which was not accounted for in the model.

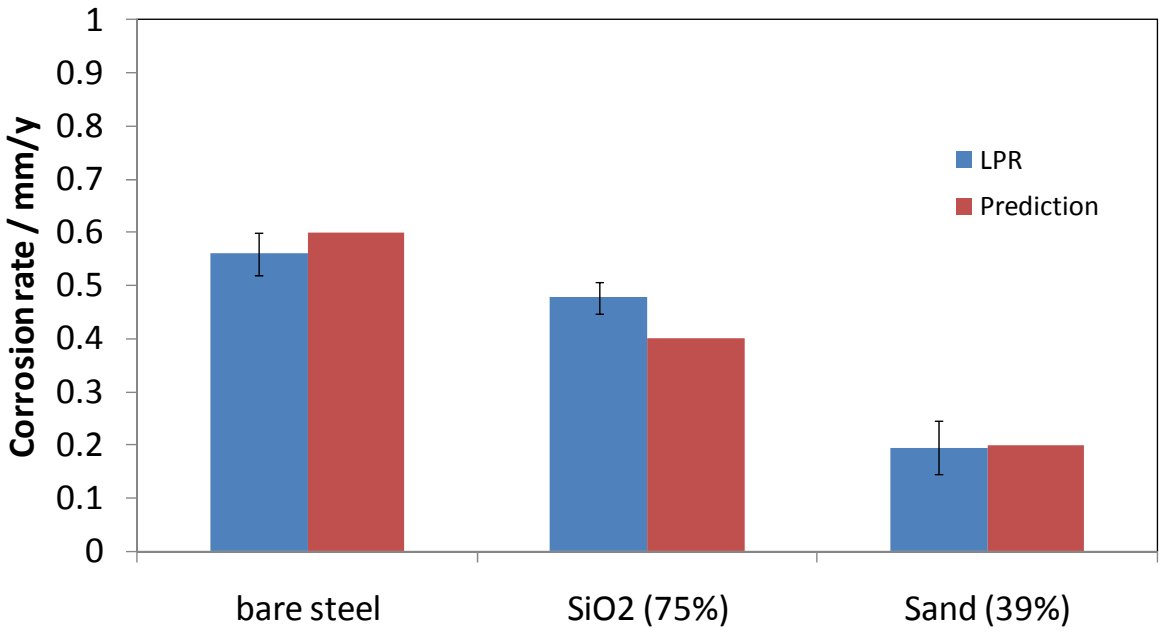

Figure 8: Comparison of predicted corrosion rate with experiment data. Experiments are conducted at pH 5, 25 °C, 1 wt% NaCl solution, $p_{CO_2} = 0.96$ bar, 2 mm deposit (porosities 75% & 39%).

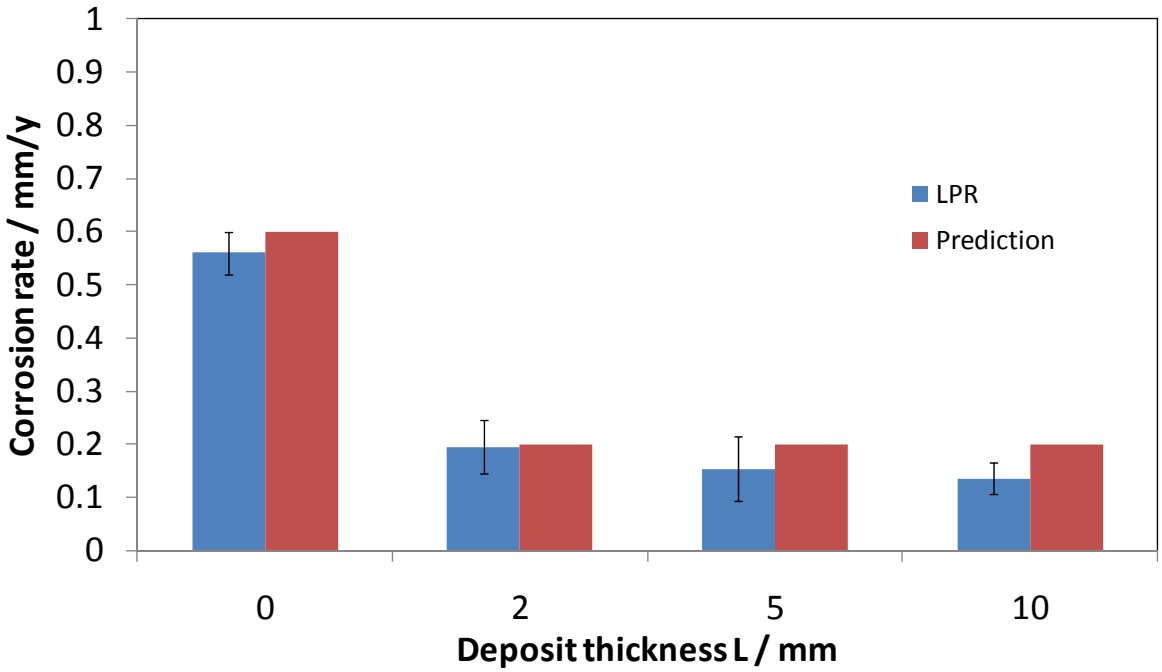

Figure 9: Comparison of predicted corrosion rate with experiment data. Experiments are conducted at pH 5, 25 °C, 1 wt% NaCl solution, $p_{CO_2} = 0.96$ bar, sand deposit porosity 39%.

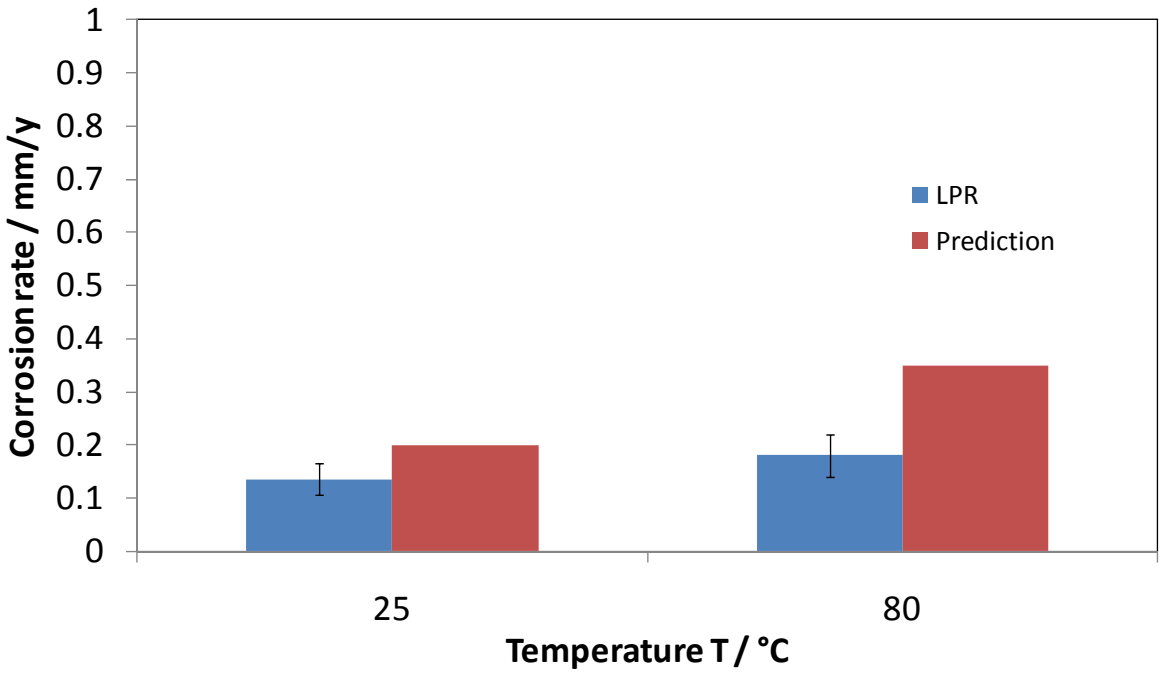

Figure 10

Figure 10: Comparison of predicted corrosion rate with experiment data at different temperature. pH 5, 25 °C, 1 wt% NaCl solution, $p_{CO_2} = 0.96$ bar, 10 mm sand deposit (porosity 39%).

CONCLUSIONS

Based on the results discussed in this work, the following conclusions were made:

1. The general corrosion rate of mild steel decreased by a factor of 3 to 5 after sand deposit was introduced, both at 25°C and 80°C;
2. Both anodic and cathodic current are decreased because of less active surface area availability due to deposit coverage.
3. The inert solid deposit creates a mass transfer barrier for corrosive species and limits cathodic reactions.
4. The extension of a simple mechanistic model can be used capture this behavior and predict the effect of a solid deposit on CO_2 corrosion of mild steel reasonably well.

ACKNOWLEDGEMENTS

The authors would like to thank the following companies for financial support: Baker Petrolite, BG Group, BP, Champion Technologies, Chevron, Clariant Oil Services, ConocoPhillips, Encana, ENI S.p.A., ExxonMobil, WGIM, Total, NALCO Energy Services, Occidental Petroleum Co., Petrobras, PETRONAS, PTT, Saudi Aramco, Inpex Corporation. Advice and comments from Professor Brian Kinsella is also greatly appreciated.

NOMENCLATURE

b_a, b_c	anodic and cathodic Tafel slope, mV/decade
Cco_2	bulk concentration of dissolved carbon dioxide, mol/m^3
D	diffusion coefficient, m^2/s
E_{rev}	reversible potential, V
F	Faradaic constant, =96485 coul/equiv.
$[H^+]_b$ $[H^+]_s$	bulk and surface concentration of H^+ (mol/m^3)
i	current density, A/m^2
i_a	activation component of the total current density, A/m^2
i_0	exchange current density, A/m^2
i^d_{lim}	diffusion limiting current density, A/m^2
i^r_{lim}	chemical reaction limiting current density, A/m^2
k^d_{CO2}	Henry's constant, mol/m^3/bar
k_m	mass transfer coefficient, m/s
L	deposit thickness, m
P_{CO2}	partial pressure of CO_2 gas, bar
R	universal gas constant, 8.314J/mol/K
t	temperature, °C
T	Kevin temperature, K
α_a, α_c,	apparent transfer coefficients
μ	viscosity, kg/m/s
κ	permeability
ψ	tortuosity
ρ	Porosity
η	= $E - E_{rev}$, overpotential, V

REFERENCES

[1] H. D. Reus, E. L. J. A. Hendriksen, and M. Wilms, "Test methodologies and field verification of corrosion inhibitors to address under deposit corrosion in oil and gas production systems", CORROSION/05, paper no. 288 (Houston, TX: NACE, 2005).

[2] D. I. Horsup, J. C. Clark, B. P. Binks, P. D. I. Fletcher, J. T. Hicks, "I put it in, but where does it go?- the fate of corrosion inhibitors in multiphase systems", CORROSION/07, paper no. 617 (Houston, TX: 2007).

[3] D. H. Pope, B. Cookingham, R. Day, G. Pogemiller, "Mitigation strategies for microbiologically influenced corrosion in gas industry facilities", CORROSION/89, paper no. 192 (Houston, TX: NACE, 1989)

[4] M. Nordsveen, S. Nesic, R. Nyborg, and A. Stangeland, "A mechanistic model for carbon dioxide corrosion of mild steel in the presence of protective iron carbonate films – part 1: theory and verification", *Corrosion* 59, 5 (2003): pp. 442 - 456A.

[5] A. Pedersen, K. Bilkova, E. Gulbrandsen, and J. Kvarekval, "CO_2 corrosion inhibitor performance in the presence of solids: test method development", CORROSION/08, paper no. 632 (Houston, TX: NACE 2008).

[6] G. Hinds, S. Zhou, Al. Turnbull and P. Cooling, "A multi-electrode approach to evaluating inhibition of underdeposit corrosion in CO_2 environments", CORROSION/09, paper no. 445 (Houston, TX: NACE, 2009).

[7] K. Lepkova and R. Gubner, “Development of standard test method for investigation of under-deposit corrosion in carbon dioxide environment and its application in oil and gas industry”, CORROSION/10, paper no. 331 (Houston, TX: NACE, 2010).

[8] M. Achour, J. Kolts, P. Humble, R. Hudgins, “Experimental evaluation of corrosion Inhibitor performance in presence of iron sulfide in CO_2/H_2S environment”, CORROSION/08, paper no. 344 (Houston, TX: NACE, 2008).

[9] S. Nesic, J. Postlethwaite, and S. Olsen, “An electrochemical model for prediction of corrosion of mild steel in aqueous carbon dioxide solutions”, *Corrosion Science* 52, 4 (1996): pp. 280-294

[10] J. Huang, B. Brown, X. Jiang, B. Kinsella and S. Nesic, “Internal CO_2 corrosion of mild steel pipelines under inert solid deposits”, CORROSION/10, paper no. 379 (Houston, TX: NACE, 2010)

[11] D. Stachewski, Chemie-Ing.-Techn., Vol. 41(1969), pp. 1.111

[12] J. O’M. Bockrts, D. Draztc, A. R. Desptc, “The electrode kinetics of the deposition and dissolution of iron”, *Electrochimica Acta* 4, 4 (1961) : p 325 - 361